Regulation of photosynthesis and oxygen consumption in a hypersaline cyanobacterial mat (Camargue, France) by irradiance, temperature and salinity

Andrea Wieland & Michael Kühl

Marine Biological Laboratory, Institute of Biology, University of Copenhagen, Helsingør, Denmark

Correspondence: Andrea Wieland, Institute of Biogeochemistry and Marine Chemistry, University of Hamburg, Bundesstr. 55, D-20146 Hamburg, Germany.
Tel.: +49 40 42838 5167;
fax: +49 40 428385167;
e-mail: wieland@geowiss.uni-hamburg.de

Received 23 May 2005; revised 19 August 2005; accepted 30 August 2005
First published online 9 November 2005.

doi:10.1111/j.1574-6941.2005.00031.x

Editor: Gary King

Keywords
microsensors; temperature; salinity; microbial mat; photosynthesis; oxygen turnover.

Abstract

Short-term effects of irradiance (0–1560 μmol photons m^{-2} s^{-1}), temperature (10–25 °C), and salinity (40–160) on oxygenic photosynthesis and oxygen consumption in a hypersaline mat (Salin-de-Giraud, France) were investigated with microsensors under controlled laboratory conditions. Dark O_2 consumption rates were mainly regulated by the mass transfer limitations imposed by the diffusive boundary layer. Areal rates of net photosynthesis increased with irradiance and saturated at irradiances > 400 μmol photons m^{-2} s^{-1}. At low irradiances, oxygen consumption increased more strongly with temperature than photosynthesis, whereas the opposite was observed at saturating irradiances. Net photosynthesis vs. irradiance curves were almost unaffected by decreasing salinity (100 to 40), whereas increasing salinities (100 to 160) led to a decrease of net photosynthesis at each irradiance. Dark O_2 consumption rates, maximal gross and net photosynthesis at light saturation were relatively constant over a broad salinity range (60–100) and decreased at salinities above the *in situ* salinity of 100. Within the range of natural variation, temperature was more important than salinity in regulating photosynthesis and oxygen consumption. At higher salinities the inhibitory impact of salinity on these processes and therefore the importance of salinity as a regulating environmental parameter increased, indicating that in more hypersaline systems, salinity has a stronger limiting effect on microbial activity.

Introduction

Light, temperature and salinity are important regulating parameters for benthic phototrophic communities growing in coastal ecosystems (e.g. Javor & Castenholz, 1984; Canfield & Des Marais, 1993; Pinckney *et al*., 1995; Garcia-Pichel *et al*., 1999; Epping & Kühl, 2000; Wieland & Kühl, 2000a, b; Hancke & Glud, 2004; Wieland *et al*., 2005). The input of organic matter by photosynthetic carbon fixation and thus also the availability of organic carbon substrates and oxygen for the heterotrophic and aerobic community in the sediment is inherently regulated by light. Temperature strongly regulates all biological processes directly via the enzymes involved and indirectly via a temperature dependency of the physico-chemical processes involved in mass transfer within the sediment and across the sediment–water interface. The latter include solute diffusion, solute solubility, water viscosity, and the thickness of the diffusive boundary layer (DBL). Whereas solute diffusion increases with temperature, the other variables decrease with temperature [Jørgensen & Revsbech, 1985; Wieland & Kühl, 2000b; Gas Tables (Unisense A/S, Denmark, http://www.unisense.dk/support/support.html)]. The DBL impedes mass transfer and controls the diffusive exchange of solutes and nutrients across the sediment–water interface, which is thus affected by temperature (Jørgensen & Revsbech, 1985; Boudreau & Jørgensen, 2001). The physico-chemical processes involved in mass transfer are also influenced by salinity, although generally to a lesser extent. Solute diffusion and solubility decrease with salinity, whereas seawater viscosity increases at higher salinities (Riley & Skirrow, 1975; Sherwood *et al*., 1991; Gas Tables, Unisense A/S, Denmark, http://www.unisense.dk/support/support.html).

Besides the natural co-variation of temperature and light, cyanobacterial mats growing in intertidal zones and in solar salterns also experience pronounced daily fluctuations of salinity (Stal, 2000). The latter is caused by water exchange in combination with pronounced sun- and wind-driven

evaporation in these shallow-water environments. Environmental salinity changes require a fast re-adjustment of the osmotic pressure within the microorganisms to avoid shrinking or osmotic bursting of the cells. Bacteria mostly regulate their osmolality by production and/or uptake of low-molecular weight organic compatible solutes to regain osmotic equilibrium with their surroundings (for review see Galinski, 1995; Roeßler & Müller, 2001). Compatible solutes are polar, highly soluble molecules, which are uncharged at physiological pH (Galinski, 1993) and which have a stabilizing effect on proteins due to their exclusion from the hydration shell of proteins (Ventosa *et al*., 1998). They do not interfere with the metabolism of the cell even at high intracellular concentrations.

In this study, we investigated finely-laminated and several centimetre-thick hypersaline cyanobacterial mats growing in a pre-concentration pond in the Salin-de-Giraud solar salt works, located on the French Mediterranean coast in the Rhône Delta (Camargue). The pond serves as a water reservoir for the salt company, fueling neighboring ponds with pre-concentrated seawater. This water exchange leads to pronounced variations of the water level and salinity in the pond (Wieland *et al*., 2005), depending on the manual operation by the salt company and prevailing climatic conditions. The pond water salinity varies between ~70 and ~100 during a diel cycle (Wieland & Kühl, 2001; Wieland *et al*., 2005). The cohesive cyanobacterial mats are dominated by *Microcoleus chthonoplastes* (Fourçans *et al*., 2004), as typically found in ponds of solar salterns with this salinity range (S = ~60–120; for review see Oren, 2000). The detailed microbial community composition with an emphasis on cyanobacteria and functional bacterial groups involved in the sulphur cycle (Fourçans *et al*., 2004), as well as the potential for biodegradation of crude oil in these mats (Benthien *et al*., 2004), were described recently. The mats are characterized by low sulphide concentrations despite very high sulphate-reduction rates, and a high iron content controls the sulphur cycle in the mats (Wieland *et al*., 2005).

We used O_2 microsensor measurements under controlled laboratory conditions to investigate the short-term regulation of oxygenic photosynthesis and oxygen consumption by irradiance, temperature and salinity, i.e. the main environmental controls on the *in situ* carbon cycle in this cyanobacterial mat community. As these key variables strongly co-vary during a diel cycle (Wieland *et al*., 2005), each parameter was changed under controlled conditions to resolve its selected impact on the mat community function *in situ*. Extrapolation of the results can help to interpret the role of key environmental parameters on microbial community activity and performance in recent and possibly also ancient coastal settings. To our knowledge, this is the first (full-factorial) study that systematically investigates and compares, with the same method, the detailed role of temperature and salinity on photosynthesis vs. irradiance curves in a single hypersaline cyanobacterial mat. Our goal was to reveal the relative importance of temperature and salinity for *in situ* carbon cycling and the physiological tolerance of the investigated benthic microbial community.

Materials and methods

Sampling

Samples of cyanobacterial mats growing in the pre-concentration pond of the Salin-de-Giraud solar salt works (Camargue, France) were taken in February 2001. *In situ* temperature and salinity at noon during sampling were 7 °C and S = 100, respectively. The mat samples were transported moist within a few hours to the Marine Biological Laboratory (Denmark).

Microsensor measurements

Mat samples were embedded in agar (1.5% w/v) and mounted in a flow chamber (Lorenzen *et al*., 1995). A constant flow of aerated artificial seawater, prepared by dissolving appropriate amounts of commercial seawater salts mixture in distilled water, was directed over the exposed mat surface with a submersible water pump (Aqua-Clear, Hagen, Holm, Germany) connected to the flow chamber. The mats were illuminated with a fiber-optic halogen light source (KL 2500, Schott, Mainz, Germany) and the temperature of the artificial seawater reservoir was adjusted with a thermostat (Julabo, Seelbach, Germany). Water salinity and temperature were measured with a refractometer (Atago, Tokyo, Japan) and a digital thermometer (Omnitherm, Omnilab, Bremen, Germany), respectively. The downwelling scalar irradiance at the mat surface, E_d, was determined with an underwater quantum irradiance meter (Biospherical Instruments, San Diego, CA).

Clark-type O_2 microsensors (Revsbech, 1989) connected to a picoammeter (UniSense A/S, Aarhus, Denmark) were operated via a motorized micromanipulator (Märzhäuser, Wetzlar, Germany; Oriel, Irvine, CA) mounted on a heavy solid stand. Microsensor signals were recorded with a strip chart recorder (Kipp & Zonen, Delft, the Netherlands) and with a PC-based data acquisition system (LabVIEW, National Instruments, Austin, TX). The O_2 microsensor had a tip diameter of 15 µm, a stirring sensitivity of ~1% and a response time, t_{90}, of ~0.3 s. The O_2 microsensor was linearly calibrated by a two-point calibration using readings of microsensor current in the air-saturated overlying water (100% air saturation) and in the anoxic part of the mat (0% O_2). Dissolved O_2 concentration of air saturated brine at experimental temperatures and salinities were calculated according to Sherwood *et al*. (1991). Gross photosynthesis

measurements with the light-dark shift method (Revsbech & Jørgensen, 1983) were done in steps of 100 μm vertical depth intervals as described in Wieland & Kühl (2000b).

At each temperature and salinity condition, measurements were started after incubating the mat in darkness overnight. After measuring dark steady-state oxygen profiles, irradiance was successively increased (0–1560 μmol photons $m^{-2} s^{-1}$). Oxygen and gross photosynthesis profiles were measured at each irradiance after reaching short-term steady-state, which was determined when multiple measurements showed no further change in the oxygen profiles under the actual experimental condition. For the temperature experiment (at the *in situ* salinity of 100), measurements were started at 10 °C and, after measuring at the selected irradiances, increased in steps of 5 °C. For the salinity experiment, one fresh mat sample was transferred into the experimental set-up and subjected to decreasing salinity, while another fresh mat sample was exposed to increasing salinity. Measurements during the salinity experiment were performed close to the *in situ* temperature at 10 °C and were started in both subsamples with the *in situ* salinity of 100, which was then either decreased or increased in salinity steps of 20. For this, either Milli-Q-water or concentrated artificial seawater was added to the artificial seawater reservoir until the desired salinity was reached, as controlled with a refractometer. After changing the temperature or salinity in the experimental set-up, mats were allowed to adjust overnight (~10 h) in darkness to the new conditions. Microsensor measurements were started the following morning with measurement of one dark steady-state oxygen profile.

Calculations

Diffusive O_2 fluxes across the mat–water interface, J_0, representing areal rates of net photosynthesis, P_n, were calculated from O_2 profiles using Fick's first law of diffusion as described in Wieland & Kühl (2000a). Areal rates of gross photosynthesis, P_g, were calculated by integration of the measured, porosity-corrected volumetric gross photosynthesis rates over the depth of the photosynthetic active zone. The mat porosity was assumed 0.9. Areal rates of O_2 consumption in light-incubated mats, R, were calculated as the difference between P_g and P_n. In dark-incubated mats, $-P_n$ represents areal rates of dark O_2 consumption, R_{dark}.

Photosynthesis versus irradiance curves (P vs. E_d curves) were obtained by fitting an exponential function (Webb *et al.*, 1974) to areal rates of gross photosynthesis at increasing irradiance by a nonlinear least-squares Levenberg-Marquardt algorithm (ORIGIN 6.0, MicroCal Software, Inc., Northampton, MA):

$$P = P_{max}[1 - \exp(-\alpha E_d(P_{max})^{-1})] \quad (1)$$

where P_{max} is the maximal photosynthetic rate at light saturation, and α is the initial slope of the P vs. E_d curve. The irradiance at the onset of photosynthesis saturation was calculated as

$$E_k = P_{max}\alpha^{-1}. \quad (2)$$

The definition and determination of the parameters and abbreviations used are listed in Table 1.

The effect of temperature on photosynthesis rates was quantified by calculating the apparent activation energy, E_a, and the factor of process rate increase by a 10 °C temperature increase, Q_{10}, according to Isaksen & Jørgensen (1996). E_a was determined from the slope of the initial linear part of an Arrhenius plot, i.e. in the temperature range below the optimum temperature of the process rate, based on the integrated form of the Arrhenius equation:

$$\ln(k) = \ln(A) + (-E_a(RT)^{-1}) \quad (3)$$

where k is the process rate, A is the Arrhenius constant, R is the gas constant (8.3144 J K^{-1} mol^{-1}) and T is the absolute temperature (K). The Q_{10} value was calculated by:

$$Q_{10} = \exp\{E_a 10[RT(T+10)]^{-1}\}. \quad (4)$$

Results

Photosynthesis and O_2 consumption as a function of irradiance and temperature

Gross photosynthesis and O_2 profiles were measured at increasing irradiance (0–1560 μmol photons $m^{-2} s^{-1}$) and temperature (10–25 °C). At 10 °C, O_2 penetration and maximal O_2 concentration within the mat gradually increased with irradiance from 0.3 mm in the dark to 1 mm at the maximal experimental irradiance (Table 2). Dark O_2 profiles were hardly affected by increasing temperature (Fig. 1) and the O_2 penetration depth was 0.25–0.30 mm at all experimental temperatures (Table 2). Both O_2 concentration and penetration depth decreased with rising temperature at low irradiances (<110 μmol photons $m^{-2} s^{-1}$), whereas at higher and saturating irradiances the maximal O_2 concentration tended to increase with temperature (Fig. 1, Table 2).

Areal rates of net photosynthesis, P_n, determined as the O_2 flux across the mat–water interface, increased with irradiance and saturated at irradiances > 400 μmol photons $m^{-2} s^{-1}$ at all experimental temperatures (Fig. 2). Dark O_2 consumption rates, R_{dark}, amounted to 0.07 nmol O_2 $cm^{-2} s^{-1}$ at 10 °C and showed only slight changes with temperature (Table 3). The compensation irradiance, E_c, i.e. the irradiance where the mat community changed from net O_2 consumption to net O_2 production ($P_n = 0$), increased strongly with temperature from 20 to 152 μmol photons $m^{-2} s^{-1}$ (Fig. 3a). Maximal net

Table 1. Definition and determination of parameters

Parameter	Definition	Determination
P_n	Areal rate of net photosynthesis (nmol O_2 cm^{-2} s^{-1})	The diffusive O_2 flux across the mat–water interface
P_g	Areal rate of gross photosynthesis (nmol O_2 cm^{-2} s^{-1})	The depth-integration of porosity-corrected volumetric rates measured with light–dark shift method (Revsbech & Jørgensen, 1983)
R	Areal rate of oxygen consumption in light (nmol O_2 cm^{-2} s^{-1})	Calculated as P_g–P_n in light-incubated mat
R_{dark}	Areal rate of dark oxygen consumption (nmol O_2 cm^{-2} s^{-1})	Calculated as $-P_n$ in dark-incubated mat
$R_{dark,vol}$	Volume-specific rate of dark oxygen consumption (nmol O_2 cm^{-3} s^{-1})	Calculated as R_{dark} × (thickness of oxic zone in darkness)$^{-1}$
P_{max}	Maximal gross photosynthesis rate at light saturation (nmol O_2 cm^{-2} s^{-1})	Determined from fit of an exponential function (Webb *et al.*, 1974) to P_g vs. irradiance data
$P_{n,max}$	Maximal net photosynthesis rate at light saturation (nmol O_2 cm^{-2} s^{-1})	Determined as the mean of P_n at light saturation (880 and 1560 μmol photons m^{-2} s^{-1})
E_c	Compensation irradiance (μmol photons m^{-2} s^{-1})	the irradiance where $P_n = 0$
E_k	Irradiance at onset of gross photosynthesis saturation (μmol photons m^{-2} s^{-1})	Calculated as $P_{max} \times \alpha^{-1}$
α	Initial slope of gross photosynthesis vs. irradiance curve (μmol O_2 μmol photons^{-1})	Calculated from fit of an exponential function (Webb *et al.*, 1974) to P_g vs. irradiance data
Z_{eff}	Thickness of effective diffusive boundary layer (DBL) (μm)	Determined from measured dark O_2 microprofiles
J_{max}	Maximal possible O_2 flux through the DBL in dark-incubated mats (assuming O_2 concentration at mat surface = 0) (nmol O_2 cm^{-2} s^{-1})	Determined as O_2 diffusion coefficient × O_2 concentration in overlying water × Z_{eff} (measured)$^{-1}$

photosynthesis rates, $P_{n,max}$, calculated as the mean of the saturated net photosynthesis rates at the highest irradiances of 880 and 1560 μmol photons m^{-2} s^{-1}, increased exponentially with temperature (Fig. 3b). An apparent activation energy of 55 kJ mol^{-1} in the temperature range between 15 °C and 25 °C was calculated (Fig. 3c), yielding a Q_{10} of 2.2 (15 to 25 °C).

Gross oxygenic photosynthesis was only measurable within the uppermost 0.3–0.7 mm of the mat (Table 2). Depth-integrated, areal gross photosynthesis rates, P_g, initially increased and then saturated at higher irradiances at all experimental temperatures (Fig. 4, left panel). At 15 °C, gross photosynthesis could not be measured at higher irradiances (> 236 μmol photons m^{-2} s^{-1}) because of intense bubble formation in the point of measurement. By fitting an exponential function (Webb *et al.*, 1974) to the areal gross photosynthesis rates at increasing irradiances, different parameters (Fig. 4, right panel) could be derived from the P vs. E_d curves (line graphs in Fig. 4, left panel). The maximal gross photosynthetic rate at light saturation, P_{max}, strongly increased with temperature from 0.35 (10 °C) to 1.09 nmol O_2 cm^{-2} s^{-1} (25 °C). An Arrhenius plot of the maximal gross photosynthetic rate at light saturation, P_{max} (Fig. 4, graph inset), showed that the major increase in rate occurred between 10 and 15 °C, indicating an optimum temperature of P_{max} close to 15 °C. Thus, the apparent activation energy, E_a, and the Q_{10} of P_{max} could not be calculated from these data.

The initial slope of the P vs. E_d curve, α, increased between 10 and 15 °C and then decreased again (Fig. 4, right panel). The photoadaptive index, E_k, i.e. the irradiance where photosynthesis starts to saturate and approaches P_{max}, increased with temperature from 127 (10 °C) to 507

Table 2. Oxygen penetration depth, maximal O_2 concentration, and depth of the photosynthesis zone at increasing experimental temperatures and irradiances (E_d)

	O_2 penetration depth (mm)				Max. O_2 concentration (μM)				Depth photosynthesis zone (mm)			
E_d (μmol photons m^{-2} s^{-1})	10 °C	15 °C	20 °C	25 °C	10 °C	15 °C	20 °C	25 °C	10 °C	15 °C	20 °C	25 °C
0	0.30	0.25	0.30	0.25	—	—	—	—	—	—	—	—
21	0.55	0.45	0.30	0.30	192	89	55	47	0.3	0.3	—	—
46	0.65	0.55	0.40	0.30	373	180	72	54	0.4	0.4	0.2	—
110	0.75	0.70	0.55	0.45	609	486	139	104	0.4	0.5	0.4	0.3
236	0.80	0.85	0.75	0.65	793	848	805	252	0.5	0.6	0.5	0.5
448	0.90	0.95	0.85	0.85	849	878	1094	1245	0.5	—	0.6	0.6
880	0.95	1.05	0.9	0.90	891	879	1089	1174	0.7	—	0.7	0.6
1560	1.00	1.10	1.00	0.95	915	894	1080	1180	0.7	—	0.7	0.7

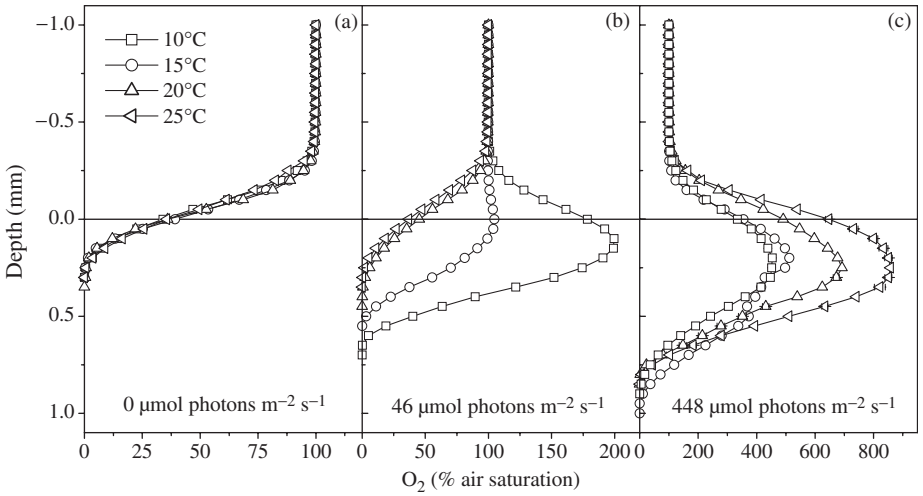

Fig. 1. Depth profiles of O_2 concentration in the Camargue microbial mat as a function of temperature at selected irradiances: (a) in darkness ($n = 1$), (b) at a low irradiance (46 µmol photons m^{-2} s^{-1}) ($n = 2$), (c) at a saturating irradiance (448 µmol photons m^{-2} s^{-1}) ($n = 1$–2). Error bars were only included if the standard deviation was higher than the range of O_2 concentration that is comprised by the symbol. Note different concentration scales. The 100% air saturation value translates into decreasing amounts of absolute O_2 concentration with increasing temperature.

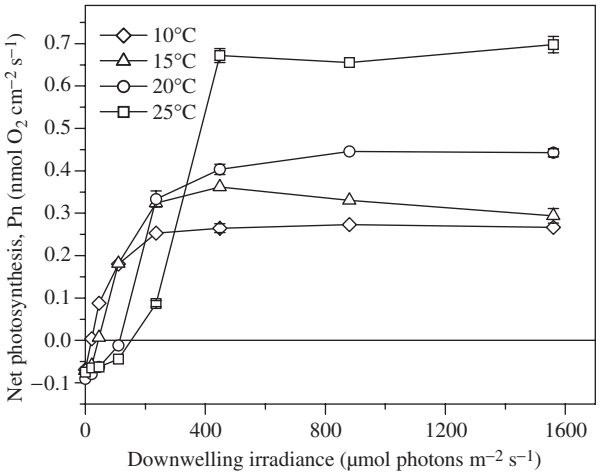

Fig. 2. Areal rates of net photosynthesis, P_n, vs. irradiance at increasing temperature, as derived from measured concentration profiles of O_2 in the Camargue microbial mat. Error bars were only included if the standard deviation was higher than the range of P_n that is comprised by the symbol.

µmol photons m^{-2} s^{-1} (25 °C). Thus, increasing irradiances were required to both initiate and saturate gross photosynthetic O_2 production at increasing temperature. The minimal irradiance where gross photosynthesis was detectable increased from 21 µmol photons m^{-2} s^{-1} (at 10 and 15 °C) to 46 and 110 µmol photons m^{-2} s^{-1} at 20 and 25 °C, respectively (Table 2).

Areal rates of oxygen consumption, R, generally increased with irradiance at all temperatures and were maximal at the highest irradiance (Table 3). Relative to P_g, R was highest at low irradiances (< 236 µmol photons m^{-2} s^{-1}) and much higher than P_g at temperatures above 10 °C. Thus, at low irradiances O_2-consuming processes increased more strongly with temperature than did photosynthesis, as already indicated by the increasing E_c with temperature (Fig. 3a). At saturating irradiances, photosynthesis increased more strongly with temperature than did O_2 consumption, as also indicated by the increasing $P_{n,max}$ with temperature (Fig. 3b).

Table 3. Areal rates of O_2 consumption (R) at increasing experimental temperatures and irradiances (E_d)

	R (nmol O_2 cm^{-2} s^{-1})				R (% of gross photosynthesis)			
E_d (µmol photons m^{-2} s^{-1})	10 °C	15 °C	20 °C	25 °C	10 °C	15 °C	20 °C	25 °C
0	0.07	0.07	0.09	0.08	—	—	—	—
21	0.07	0.10	—	—	95	232	—	—
46	0.05	0.13	0.09	—	37	95	307	—
110	0.02	0.16	0.13	0.09	12	47	110	200
236	0.01	0.21	0.22	0.19	5	39	40	68
448	0.03	—	0.36	0.20	10	—	47	23
880	0.07	—	0.38	0.20	20	—	46	23
1560	0.14	—	0.57	0.33	34	—	56	32

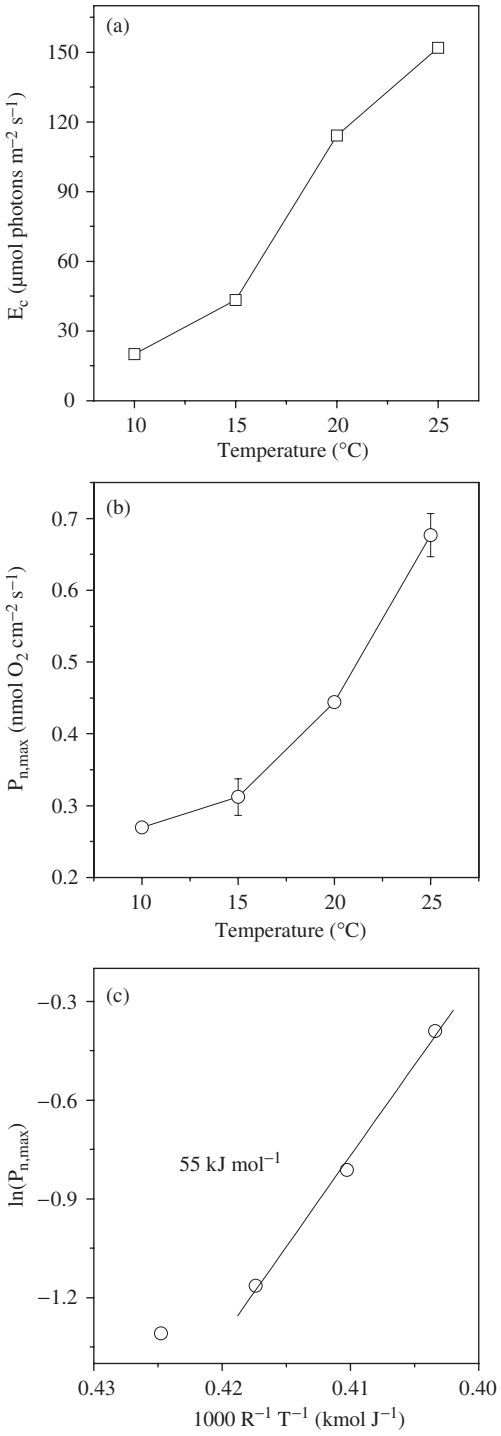

Fig. 3. Compensation irradiance, E_c (a), and maximal net photosynthesis, $P_{n,max}$ (b) at increasing temperatures as determined from the data shown in Fig. 2. Error bars show standard deviation of the mean of saturated net photosynthesis rates at the highest irradiances of 880 and 1560 µmol photons m^{-2} s^{-1}, representing $P_{n,max}$. (c) Arrhenius plot of the rates of $P_{n,max}$ shown in (b).

Photosynthesis and O_2 consumption as a function of irradiance and salinity

In two subsamples of the same mat, gross photosynthesis and O_2 profiles were measured as a function of salinity and irradiance, using the same irradiances as above except at 880 µmol photons m^{-2} s^{-1}.

The oxygen penetration depth increased with irradiance at all salinities and showed a decreasing trend at a given irradiance when salinity was increased or decreased above/below $S = 100$ (Fig. 5, Table 4). The maximal O_2 concentration and the depth of the photosynthetic active zone increased with irradiance, but did not show a clear trend with salinity. However, the maximal O_2 concentration in the mat (at a given irradiance) showed a decreasing trend with increasing salinity at salinities >100 (Table 4).

Areal rates of net photosynthesis increased with irradiance and saturated at irradiances >400 µmol photons m^{-2} s^{-1} at all salinities (Fig. 6). P_n vs. E_d curves were almost unaffected by decreasing salinity (Fig. 6a). Only at $S = 40$ did a slight decrease of P_n occur at low irradiances. In contrast, increasing salinity led to a change in the shape of the P_n vs. E_d curves, and at each experimental irradiance P_n decreased with increasing salinity (Fig. 6b). Thus, maximal net photosynthesis rates, $P_{n,max}$, decreased at salinities above the *in situ* salinity, whereas at lower salinities $P_{n,max}$ varied only slightly (Fig. 7c).

Dark O_2 consumption rates, R_{dark}, normalized to the corresponding rate at $S = 100$, were relatively constant over a broad salinity range (60–120). However, R_{dark} increased strongly at $S = 40$, whereas at salinities of 140 and 160, R_{dark} decreased to almost half the rate at $S = 100$ (Fig. 7a). The compensation irradiance, E_c, was lowest at $S = 100$ and increased with increasing and decreasing salinity (Fig. 7b).

Except at $S = 160$, gross photosynthesis profiles were measured at each experimental condition and the data sets of depth-integrated gross photosynthesis rates vs. irradiance were analyzed as described above (data not shown). As derived from these curves, the maximal gross photosynthesis rate at light saturation, P_{max}, was relatively constant over a broad salinity range ($S = 40$–100) and only decreased at salinities higher than the *in situ* salinity (Fig. 8a). Neither α nor E_k showed a clear trend with salinity (Fig. 8b, c). As gross photosynthesis could not be measured at the highest irradiance at $S = 120$ because of air bubble formation, P_{max} and E_k are underestimated at this salinity.

Temperature and salinity effects on the diffusive boundary layer and R_{dark}

Based on the measured thickness of the effective diffusive boundary layer, Z_{eff}, in the dark-incubated mats at 10 °C and $S = 40$, respectively, we calculated the relative theoretical

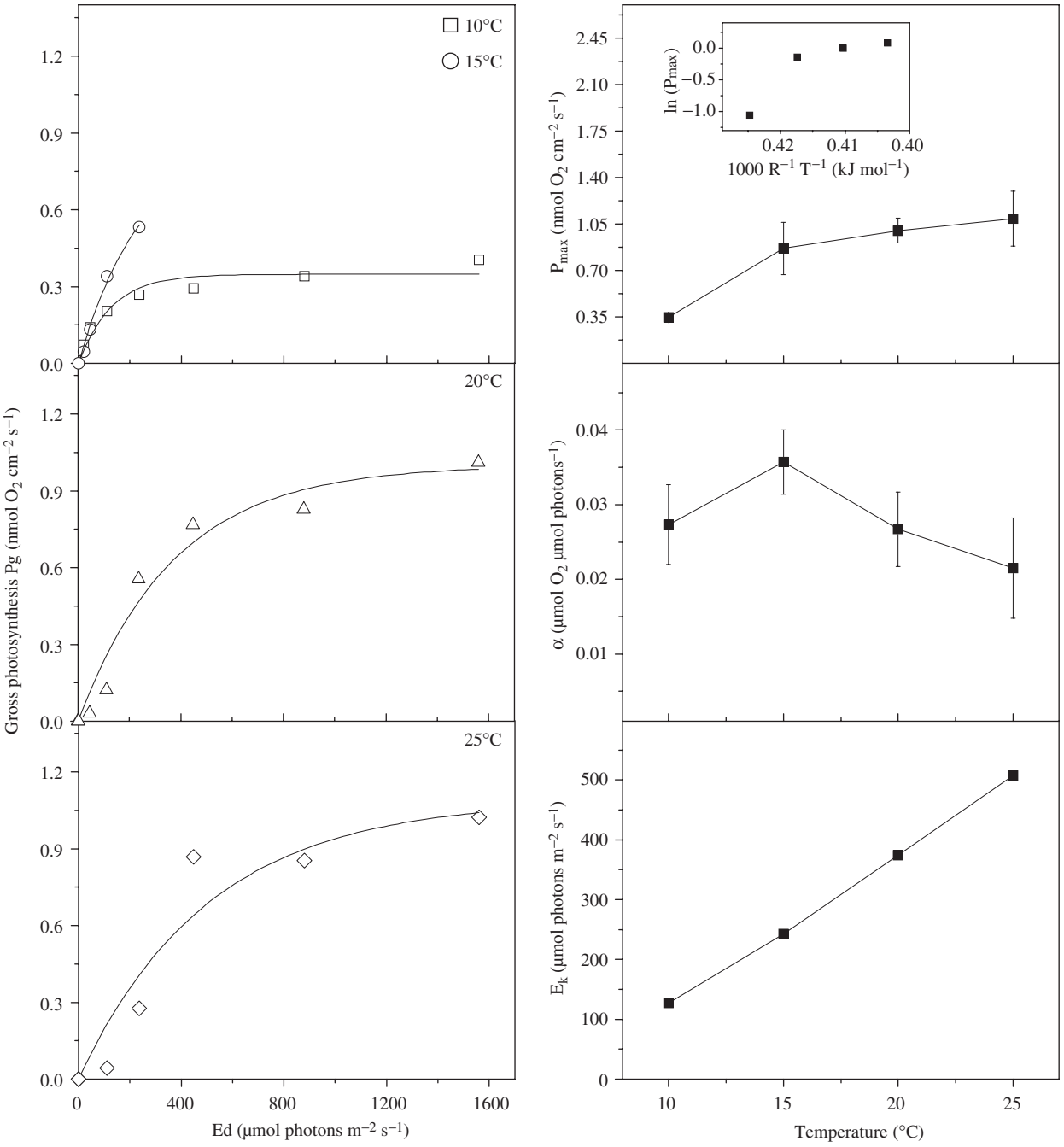

Fig. 4. Areal rates of gross photosynthesis, P_g, vs. irradiance, E_d, at increasing temperatures (left panel). Line graphs show fits of an exponential function to the data sets. Maximal gross photosynthesis, P_{max}, the initial slope of the curves, α, and the irradiance at onset of saturation of photosynthesis, E_k, vs. temperature (right panel). Graph inset shows Arrhenius plot of P_{max}.

change of Z_{eff} with temperature and salinity as described in Garcia-Pichel *et al.* (1999). Furthermore, the maximal possible O_2 flux through the DBL in the dark-incubated mats, J_{max}, was calculated from this data set (Table 1) according to Garcia-Pichel *et al.* (1999) and Wieland & Kühl (2000b).

The effective thickness of the DBL would theoretically decrease 17% between 10 °C and 25 °C if only the effects of temperature on physico-chemical parameters such as water density and dynamic viscosity are considered (Fig. 9a). Thus, as calculated from the measured $Z_{eff} = 239\,\mu m$ at 10 °C in the dark-incubated mat, Z_{eff} should theoretically decrease to 199 µm at 25 °C. Except at 25 °C, the predicted and measured thicknesses of the DBL were in good agreement at all temperatures. In contrast, at increasing

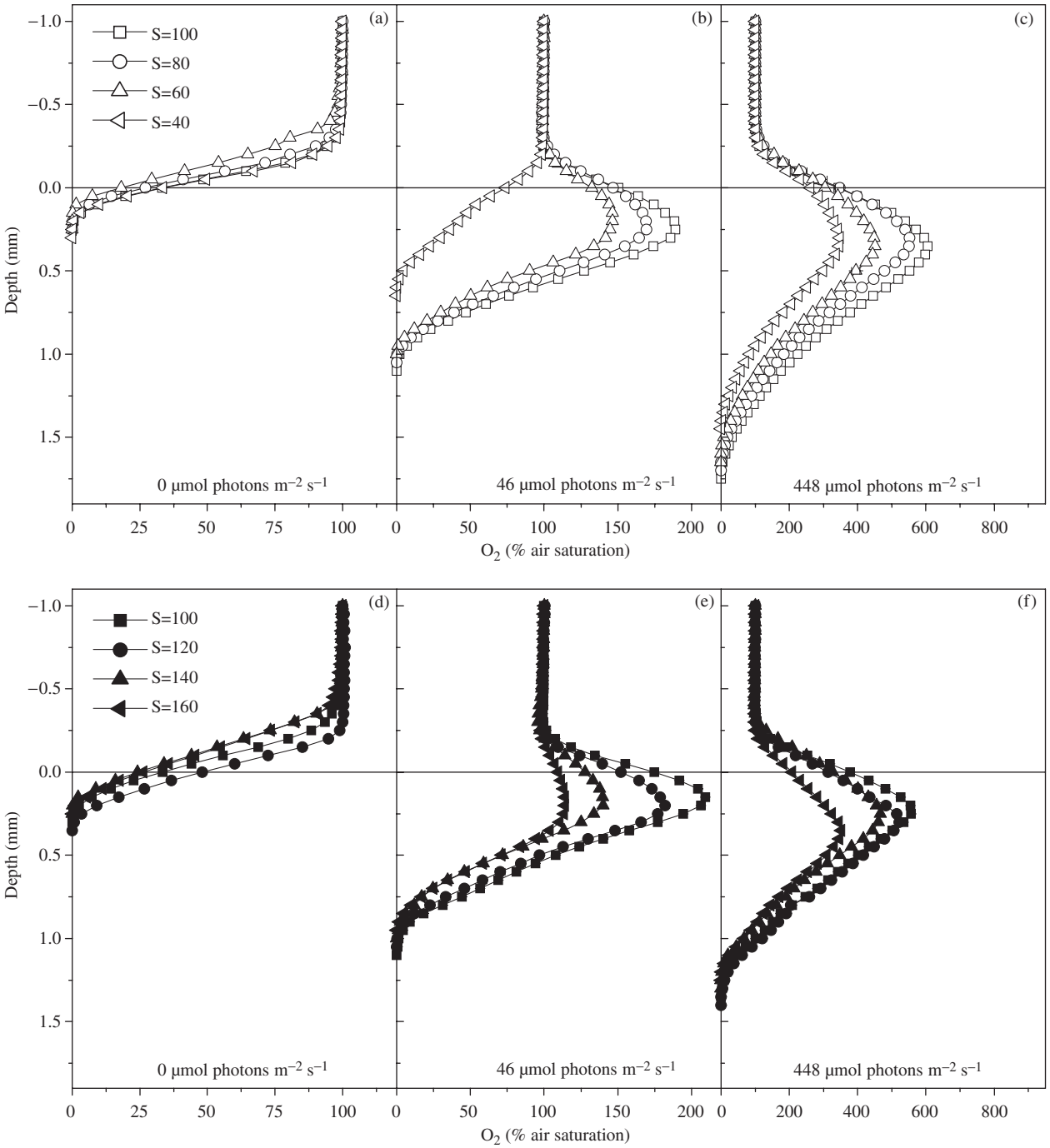

Fig. 5. Depth profiles of O_2 concentration in the Camargue microbial mat as a function of salinity at selected irradiances: (a), (d) in darkness ($n = 1$), (b), (e) at a low irradiance (46 µmol photons m^{-2} s^{-1}) ($n = 2$), (c), (f) at a saturating irradiance (448 µmol photons m^{-2} s^{-1}) ($n = 2$–3). Error bars were only included if the standard deviation was higher than the range of O_2 concentration that is comprised by the symbol. Note different concentration scales. The 100% air saturation value translates into decreasing amounts of absolute O_2 concentration with increasing salinity.

salinities, the measured Z_{eff} differed strongly from the theoretical Z_{eff} (Fig. 9b). Theoretically, Z_{eff} should increase linearly from the measured DBL thickness at $S = 40$ of 199 µm to 212 µm at $S = 160$, corresponding to an increase of 6%. However, the measured Z_{eff} was mostly much higher than the theoretical Z_{eff}, with a maximal thickness of 384 µm at $S = 140$.

At all temperatures, the measured R_{dark} were lower than J_{max} (Fig. 9c), with a relatively constant difference of ~33–36% (relative to J_{max}). Taking the DBL thickness at

Table 4. Oxygen penetration depth, maximal O_2 concentration, and depth of the photosynthesis zone at the experimental salinities and irradiances (E_d)

	O_2 penetration depth (mm)				Max. O_2 concentration (μM)				Depth photosynthesis zone (mm)			
E_d (μmol photons m^{-2} s^{-1})	$S = 100$	80	60	40	$S = 100$	80	60	40	$S = 100$	80	60	40
0	0.25	0.20	0.15	0.25	—	—	—	—	—	—	—	—
21	0.80	0.60	0.45	0.35	183	134	86	68	0.5	0.4	0.2	0.1
46	1.05	1.05	1.00	0.60	351	360	356	204	0.5	0.5	0.5	0.3
110	1.40	1.35	1.30	1.10	627	674	706	548	0.6	0.6	0.6	0.5
236	1.65	1.50	1.55	1.35	888	950	1015	837	0.7	0.6	0.6	0.6
448	1.70	1.65	1.60	1.45	1125	1174	1097	959	0.7	0.7	0.7	0.7
1560	1.80	1.75	1.65	1.50	1295	1191	1081	960	0.9	0.9	0.9	0.9
E_d (μmol photons m^{-2} s^{-1})	$S = 100$	120	140	160	$S = 100$	120	140	160	$S = 100$	120	140	160
0	0.25	0.35	0.20	0.25	—	—	—	—	—	—	—	—
21	0.85	0.85	0.65	0.45	219	183	116	72	0.3	0.4	0.3	n.d.
46	1.10	1.00	1.00	0.95	392	295	197	139	0.4	0.4	0.4	n.d.
110	1.15	1.15	1.05	1.10	624	468	348	233	0.4	0.5	0.5	n.d.
236	1.25	1.25	1.15	1.15	848	671	487	332	0.5	0.5	0.5	n.d.
448	1.35	1.35	1.25	1.25	1041	846	657	429	0.5	0.6	0.5	n.d.
1560	1.50	1.65	1.45	1.35	1293	592	946	611	0.7	—	0.7	n.d.

10 °C and calculating the maximal O_2 flux through the DBL at increasing temperatures with the theoretical change of Z_{eff} (Fig. 9a) (and not the measured change as for J_{max}, see Table 1), the maximal O_2 flux through the DBL would theoretically increase linearly with temperature by 41% (J_{max} (theoretical)). At increasing salinities, the difference between J_{max} and R_{dark} varied between 20 and 49% (Fig. 9d). The theoretical decrease of the maximal O_2 flux through the DBL, taking only the effects on physical parameters into account, J_{max}(theoretical), amounts to 66% between salinities of 40 and 160.

Thus, at increasing temperatures, Z_{eff} and probably also R_{dark} are mainly controlled by the temperature effects on the physico-chemical parameters determining the O_2 flux across the DBL, whereas at increasing salinities, effects on the activity and probably also the surface topography of the mat community had a stronger impact on both parameters.

Discussion

Regulation of photosynthesis and O_2 consumption by temperature and irradiance

The distribution of O_2 and oxygenic photosynthesis (Table 2) is in accordance with the micro-optical properties of the Camargue microbial mats. Measurements of spectral scalar irradiance in this mat showed that PAR was only available within the uppermost millimeter of the mat (Fourçans *et al.*, 2004), i.e. the zone where photosynthesis occurred under all experimental conditions applied.

The maximum temperature of 25 °C applied in the experiments is well within the range of temperatures experienced by the microbial mat community in its natural habitat. *In situ* measurements over a diel cycle in May 2000 (Wieland & Kühl, 2001) and June 2001 (Wieland *et al.*, 2005) showed daily variations of 16–32 °C ($S = 75$–109) and 11–25 °C ($S = 72$–94), respectively. However, the *in situ* temperature at noon during sampling in February 2001 was only 7 °C. Thus, the lower ambient temperatures and probably also less pronounced daily temperature variations in winter could have resulted in an adaptation of the microbial community to lower temperatures. Our results should therefore be regarded as maximal temperature effects.

The finding of a minor temperature dependence of dark O_2 consumption rates is consistent with results obtained in a hypersaline cyanobacterial mat from Solar Lake (Sinai, Egypt) (Wieland & Kühl, 2000a,b). An almost unchanged O_2 penetration depth during dark incubation (Table 2) indicates that increasing temperature did not lead to an enhancement of O_2 consumption by organotrophic respiration and sulphide oxidation, which mainly determine R_{dark} in marine microbial mats. As sulphate reduction in the mats is strongly influenced by the daily temperature variations (Wieland *et al.*, 2005), the high iron content of the mat seems to have buffered a temperature-enhanced sulphide production.

The effects of temperature on mass transfer include increasing diffusion coefficient and decreasing solubility, water viscosity and thickness of the effective DBL with temperature. In the range from 10 to 25 °C, the molecular O_2 diffusion coefficient increased by 54%, whereas the O_2 solubility decreased by 24%, the kinematic viscosity of the seawater (dynamic viscosity/density) by 31% and the

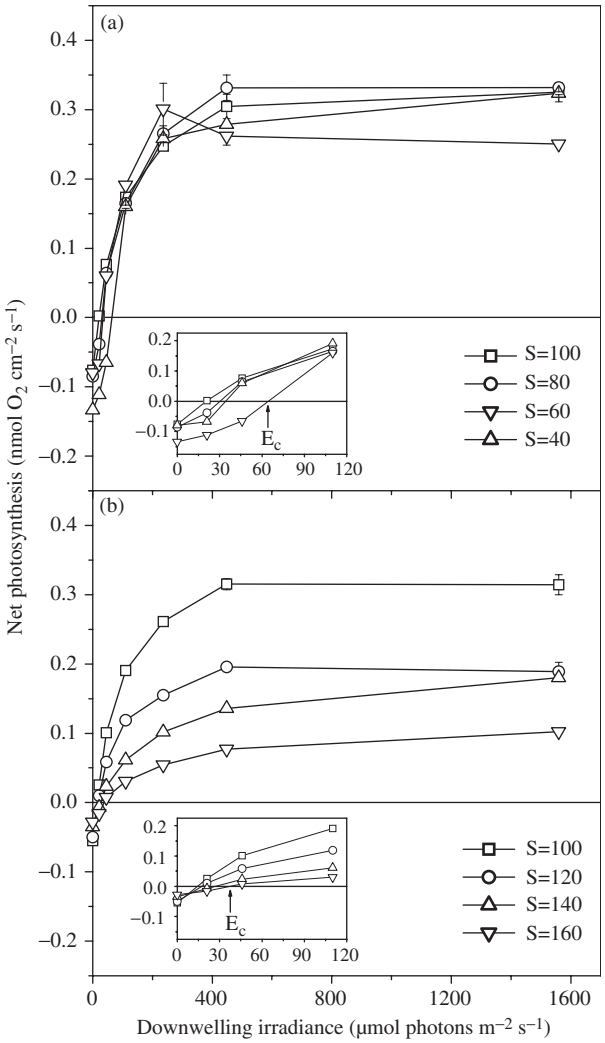

Fig. 6. Areal rates of net photosynthesis vs. irradiance at decreasing (a) and increasing (b) salinity as derived from measured concentration profiles of O_2 ($n = 1$ in dark and $n = 2$–3 in light incubations) in the Camargue microbial mat. Error bars were only included if the standard deviation was higher than the range of P_n that is comprised by the symbol. Areal net photosynthesis rates at irradiances < 120 µmol photons m^{-2} s^{-1} are shown in more detail within the graph insets.

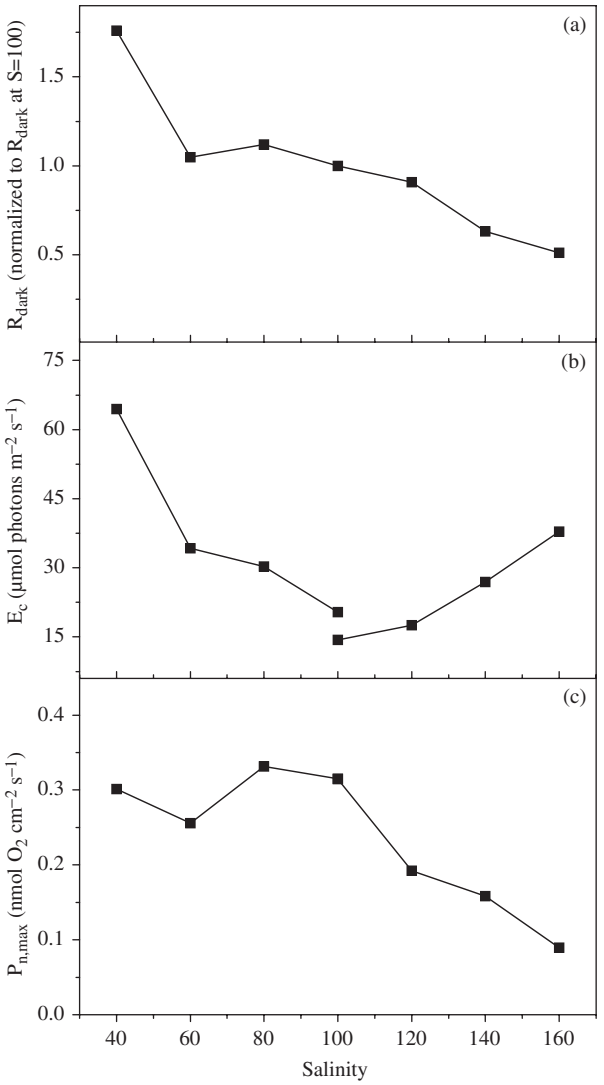

Fig. 7. Areal dark O_2 consumption rates, R_{dark}, normalized to the rate of R_{dark} at $S = 100$ (a), compensation irradiance, E_c (b), and maximal net photosynthesis, $P_{n,max}$ (c) at increasing salinity as determined from the data shown in Fig. 6.

theoretical DBL thickness, Z_{eff}(theoretical), by 17% (Fig. 9). The O_2 flux through the DBL should therefore be enhanced by the increasing diffusion coefficient and decreasing DBL thickness, which is slightly counterbalanced by the decreasing O_2 solubility. R_{dark} increased only by 9% between 10 and 25 °C, with a relatively constant difference between R_{dark} and J_{max} at all temperatures (Fig. 9). Furthermore, changes of Z_{eff}(measured) at 20 and 25 °C, e.g. by temperature-induced changes of surface topography, apparently also influenced R_{dark} at these temperatures (Fig. 9). Thus, R_{dark} is strongly controlled by the diffusive mass transfer limitations imposed by the DBL (Jørgensen & Des Marais, 1990), resulting in a low temperature-dependence of R_{dark}.

Correcting the oxygen fluxes into the mat during darkness, R_{dark}, for the oxygen penetration depth at the corresponding temperatures, a volume-specific rate of dark oxygen consumption, $R_{dark,vol}$, is obtained, representing solely the response of the microbial community to increasing temperature. In diatom-dominated benthic communities from temperate and high-arctic subtidal sites, $R_{dark,vol}$ exhibited a much higher temperature dependency (Q_{10}) than R_{dark}. This was ascribed to an underestimation of the microbial temperature response by R_{dark} due to a decreasing thickness of the oxic zone with increasing temperature (Hancke & Glud, 2004). A similar trend can also be

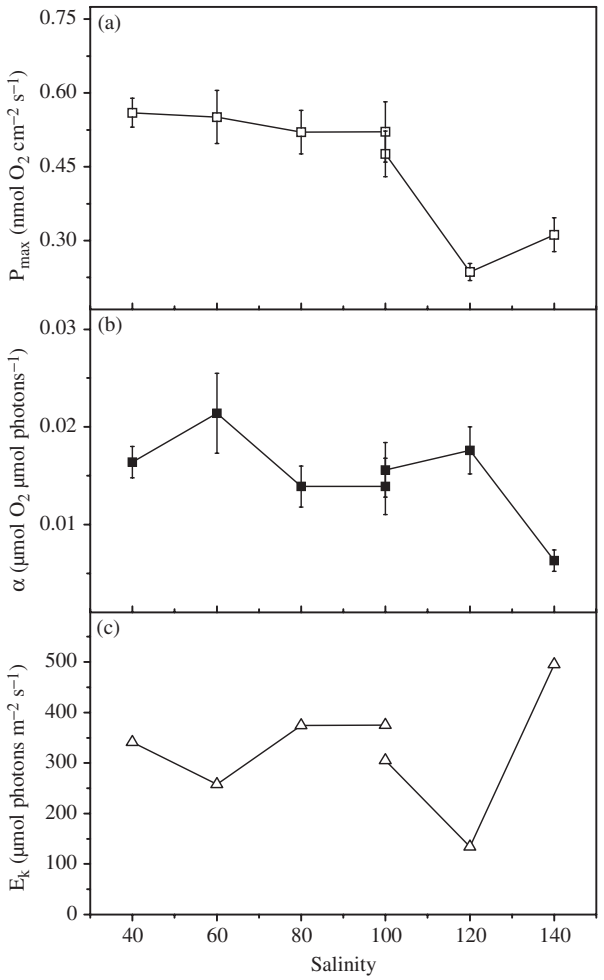

Fig. 8. Areal rates of maximal gross photosynthesis, P_{max} (a), the initial slope of the curves, α (b), and the irradiance at onset of saturation of photosynthesis, E_k (c), at increasing salinity, as determined from fits of an exponential function to measured gross photosynthesis vs. irradiance curves.

found for hypersaline cyanobacterial mats, comparing the Q_{10} of $R_{dark,vol}$ of 2.35 for mats from the Ebro Delta (Spain) (Epping & Kühl, 2000) and of R_{dark} of 1.3 for mats from Solar Lake (Egypt) (Wieland & Kühl, 2000a), respectively. However, in the Camargue microbial mat the oxygen penetration depth in dark-incubated mats and R_{dark} did not change significantly with temperature (Fig. 1, Tables 2, 3), resulting in volume-specific rates, $R_{dark,vol}$, of 2.3, 2.9, 3.0 and 3.0 nmol O_2 cm^{-3} s^{-1} at 10, 15, 20 and 25 °C, respectively, and a Q_{10} of 1.3 for $R_{dark,vol}$ between 10 and 20 °C. Thus, in the Camargue microbial mat, the microbial community is already diffusion-limited at 10 °C, leading to a low temperature dependency of dark oxygen consumption in this mat.

Photosynthesis was strongly regulated by temperature at all experimental irradiances (Figs 2–4). At light saturation, photosynthesis rates are mainly controlled by the carbon metabolism. The temperature-induced increase of maximal gross photosynthesis, P_{max} (Fig. 4), can therefore mainly be ascribed to the temperature dependence of enzymatic reactions of the Calvin cycle and inorganic carbon diffusion (Davison, 1991; Henley, 1993). This increase of gross O_2 production was not accompanied by an increase of O_2 consumption, as maximal net photosynthesis rates, $P_{n,max}$, also increased with temperature (Fig. 3). In terms of O_2 production, the productivity of the mat was thus highest at elevated temperatures and irradiances, comparable to *in situ* conditions prevailing during the afternoon (Wieland *et al.*, 2005).

The Q_{10} of 2.2 for maximal net photosynthesis rates, $P_{n,max}$, is well within the range of Q_{10} values (of ~2) found for photosynthesis (Davison, 1991). The strong increase of P_{max} between 10 and 15 °C indicates that at 10 °C P_{max} was limited by temperature, whereas at increasing temperature (above the optimum temperature at ~15 °C) high rates of gross photosynthesis became limited by other parameters such as the availability of CO_2 for photosynthetic carbon fixation.

At low irradiances, increasing temperature led to a decrease of gross photosynthesis, as expressed by the increasing threshold irradiance, i.e. the lowest irradiance leading to detectable gross photosynthetic O_2 production (Table 2). Furthermore, the irradiance where photosynthesis starts to saturate, E_k, increased strongly with temperature (Fig. 4). Thus, increasing irradiances were required to initiate and saturate photosynthesis. Photosynthesis at low irradiances is light-limited and thus in general controlled by light-harvesting efficiency and photochemical reactions. These factors [and therefore α (Fig. 4)] are not directly regulated by temperature (Davison, 1991) and other processes must have influenced the photosynthetic performance at light-limitation. Because of the low *in situ* sulphide concentrations (Wieland *et al.*, 2005) and the almost unchanged dark O_2 profiles at increasing temperatures (Fig. 1), the possibility of cyanobacterial anoxygenic photosynthesis at low irradiances induced by temperature-increased sulphide levels (see Epping & Kühl, 2000; Wieland & Kühl, 2000a) can probably be excluded. Since cyanobacteria share components of the respiratory and photosynthetic electron transport chain (Peschek, 1999), these interactions might have caused the observed strong reduction or even suppression of photosynthesis by increased cyanobacterial respiration.

In cyanobacteria, the respiratory electron transport is significantly enhanced by heat stress (defined as 5–10 °C higher than cultivation temperature), thereby suppressing the activity of the photosynthetic electron transport (Lajkó *et al.*, 1997). Relative to photosynthesis, oxygen consumption at low irradiances was stimulated by temperature (Table

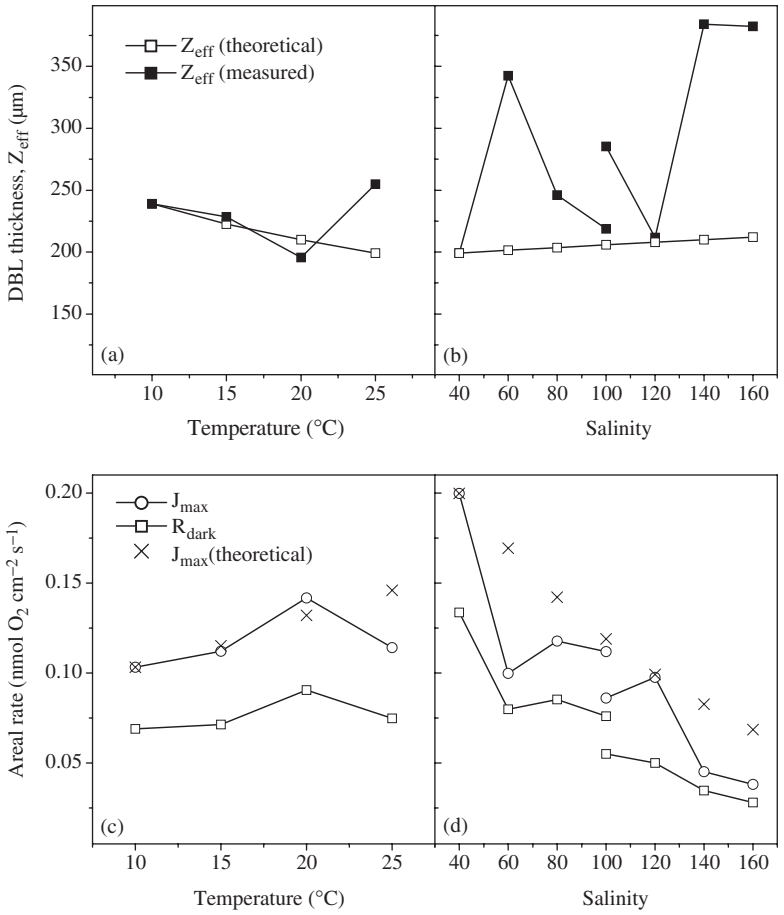

Fig. 9. Theoretical, Z_{eff}(theoretical), and measured, Z_{eff}(measured), thickness of the effective diffusive boundary layer (DBL) at increasing temperature (a) and salinity (b). Areal rates of dark O_2 consumption, R_{dark}, the maximal possible O_2 flux through the DBL, J_{max}, and the maximal theoretical O_2 flux, J_{max}(theoretical), in the dark-incubated mats at increasing temperature (c) and salinity (d).

3), causing the increasing compensation irradiance, E_c, with temperature (Fig. 3), as observed previously in hypersaline cyanobacterial mats (Epping & Kühl, 2000; Wieland & Kühl, 2000a). Thus, enhancement of cyanobacterial respiration could explain our data on light-limited oxygenic photosynthesis at increasing temperature. However, in the natural environment, decreasing irradiances are accompanied by decreasing temperatures and *vice versa* (Wieland *et al.*, 2005), thereby balancing the effects of light and temperature on photosynthesis during the diel cycle.

Regulation of photosynthesis and O_2 consumption by salinity and irradiance

Within the range of natural variations, O_2 cycling in the Camargue microbial mat was less strongly affected by changes in salinity. Significant changes occurred especially at salinities higher than the *in situ* salinity (> 100), pointing to an increasing importance of salinity as a regulating and limiting environmental parameter in more saline systems.

Increasing salinity requires active extrusion of salt from the cell cytoplasm and production and/or uptake of organic compatible solutes by the microorganisms to increase their cytoplasmic turgor and regain osmotic equilibrium with their surroundings. Transport systems for glycosylglycerol, the major osmolyte in moderately halotolerant cyanobacterial strains, and glycine betaine, the osmoticum of the most salt tolerant cyanobacteria, have been described (Joset *et al.*, 1996; Oren, 2000 and references therein). Furthermore, an active sodium ion extrusion system in cyanobacteria has been indicated (reviewed in Joset *et al.*, 1996). The production or uptake of these osmoprotective compounds is energetically expensive (Oren, 1999), with uptake being preferred over *de novo* synthesis (Galinski & Trüper, 1994; Ventosa *et al.*, 1998).

In cyanobacteria, increasing salinity ('salt upshock') leads to enhancement of respiration rates and can cause a temporary depression of photosynthesis, which, however, recovers after several hours (reviewed in Oren, 2000). In the Camargue microbial mat, R_{dark}, P_n and P_{max} decreased at salinities higher than the *in situ* salinity ($S > 100$) (Figs 6–8), which probably would have continued at further increasing salinities ($S > 160$). Thus, increasing salinity may have directly affected the microorganisms and their metabolic activity, e.g. by causing significant water loss or

increased intracellular salt concentrations. Salinity varies between ~70 and ~100 in the natural environment, and the microbial mat community was apparently not adapted to further increasing salinity and could not compensate the increased energy demands to maintain osmotic equilibrium (via salt extrusion and uptake/production of osmolytes) by increased rates of respiration (Oren, 2000) or photosynthesis (Joset *et al.*, 1996). Thus, the salinity-dependent limitation of metabolic processes becomes more important at higher salinities, indicating that in more saline systems than the investigated Camargue mats, salinity has a leading role as controlling environmental factor (see also below). Paerl *et al.* (2003) found that hypersalinity in the range of > 5 times seawater salinity is highly inhibitory for photosynthesis and nitrogen fixation and thus for mat growth. A natural reduction of salinity by increased freshwater input from hurricanes and large storms alleviated salt inhibition and led to an enhancement of the productivity of mats growing in hypersaline Bahamian lakes, thereby serving as excellent indicators of climatic and ecological changes in these water-stressed environments (Paerl *et al.*, 2003).

Decreasing salinity necessitates extrusion and/or catabolism of osmolytes, including their conversion into osmotically inactive forms, to avoid osmotic bursting of the cells (Galinski & Trüper, 1994). These mechanisms and especially their extrusion into the surroundings, possibly by transient permeability changes of the cell membrane (Reed *et al.*, 1986), may not be as costly for the cells as the uptake/synthesis of osmolytes or active salt extrusion. It was shown that extrusion of osmolytes upon decreasing salinity is fast (within minutes) in cyanobacteria (reviewed in Galinski, 1995; Joset *et al.*, 1996). As R_{dark} hardly changed when salinity was decreased from 100 to 60 (Fig. 7), extruded osmolytes apparently did not serve as an additional substrate, e.g. for aerobic heterotrophic bacteria or cyanobacteria (Oren, 1990; Sørensen *et al.*, 2004).

In the pre-concentration pond of the Salin-de-Giraud salterns, salinity increased during a diel cycle from 70 to 100 caused by water exchange with adjacent ponds (Wieland *et al.*, 2005). Our data indicate that it was mainly the range of natural salinity variations, rather than the energetic aspects, that determined the response of the microbial community to salinity changes. In this natural range, both photosynthesis and O_2 consumption were relatively stable and only decreased/increased at salinities above or below it (Figs 6–8). Within the range of *in situ* salinities, the microbial community is thus well adapted to short-term salinity fluctuations. This is in agreement with the findings of Karsten (1996), who showed that several isolated strains of the mat-building cyanobacterium *M. chthonoplastes* possess a genetically fixed growth preference for the range of salinities at their habitat, leading to the development of different physiological ecotypes. We speculate that this could also be the case for other major functional groups, resulting in the development of 'mat-ecotypes'. This could lead to different responses of microbial mat communities growing in hypersaline habitats to changes of environmental parameters, as determined by the natural variability of irradiance, temperature, and salinity at their habitat *in situ*.

Besides direct salinity effects on the microbial community, indirect effects of salinity also seem to play an important role in the regulation of microbial activity in hypersaline microbial mats (Garcia-Pichel *et al.*, 1999). Within the range of salinities applied in this study ($S = 40$–160), oxygen diffusion and solubility decreased by 17% and 56%, whereas the kinematic viscosity increased by 13% and Z_{eff}(theoretical) in the dark-incubated mats by 6% (Fig. 9). Thus, the minor increase of the DBL thickness and the decrease of O_2 diffusion, and especially solubility, should (also without activity changes of the microbial community) lead to decreasing O_2 fluxes in the dark-incubated mats with increasing salinity. This was indeed observed for the overall salinity range applied in this study (Fig. 9). Increasing salinity caused strong variations of DBL thickness (Fig. 9), influenced by changes in the surface topography due to migration of cyanobacteria and exopolymer formation. These variations also influenced the salinity response of R_{dark}, as an increasing DBL thickness due to a more pronounced mat surface topography may lead to lower O_2 fluxes across the mat–water interface and *vice versa* (Jørgensen & Des Marais, 1990).

Salinity-dependent intensification of diffusive mass transfer limitations (Garcia-Pichel *et al.*, 1999) could explain decreasing dark O_2 consumption and photosynthesis rates with increasing salinity (Figs 7, 8). A general trend of increasing photosynthetic activity (and partly also oxygen consumption rates) with experimentally decreasing salinity, and *vice versa*, has been observed for different microbial mat communities growing in diverse hypersaline environments (Pinckney *et al.*, 1995; Garcia-Pichel *et al.*, 1999; Canfield *et al.*, 2004; Sørensen *et al.*, 2004). Furthermore, a comparison of different mats growing along a salinity gradient in a Mexican solar saltern also showed decreasing gross photosynthetic oxygen production with increasing brine salinity (Des Marais *et al.*, 1989; Kühl *et al.*, unpublished data). Similar observations, i.e. decreasing photosynthetic carbon fixation at increasing salinities, were found for phytoplankton in different ponds along a salinity gradient in a Spanish solar saltern (Joint *et al.*, 2002), pointing to a general salinity-dependent limitation of oxygenic photosynthesis (and oxygen-consuming processes) at elevated salinities (Garcia-Pichel *et al.*, 1999).

In the Camargue microbial mat, both dark O_2 consumption and photosynthesis rates decreased at salinities above the *in situ* salinity (Figs 7, 8), but the almost constant rates of R_{dark}, $P_{n,max}$ and P_{max} over a relatively broad salinity range

and the absence of an overall trend of increasing gross photosynthesis with decreasing salinity (see above) contradicts a predominant role of salinity-induced changes of physico-chemical parameters and mass transfer in the Camargue microbial mats. Such limiting effects are more important at higher salinities than those we applied in our experiments (see also below). Despite a certain contribution of salinity effects on physico-chemical parameters and mass transfer (Fig. 9), the short-term response of the Camargue microbial mat community to salinity changes was governed rather by an effective adaptation of the microbial community to their natural salinity range. According to Golubic (1980), environments with fluctuating salinity select for halotolerance (and euryhalinity).

Environmental control of photosynthesis in hypersaline cyanobacterial mats

In accordance with Skyring & Bauld (1990) our data show that light is the environmental factor of central importance for phototrophic mat communities. These authors also concluded that with the exception of light, water activity in its various manifestations probably exerts the most significant environmental control on phototrophic microbial communities in coastal habitats. This was supported by several studies showing that increasingly hypersaline conditions result generally in lower productivity of microbial mat communities (e.g. Des Marais *et al*., 1989; Pinckney *et al*., 1995; Garcia-Pichel *et al*., 1999; Paerl *et al*., 2003; Canfield *et al*., 2004; Sørensen *et al*., 2004) and that this stress may outweigh the typical limiting factors regulating phototrophic community primary production, growth and function (Pinckney *et al*., 1995). Thus, our data on decreasing photosynthesis at salinities above the *in situ* salinity (>100) also support the finding of an increasing and finally overriding role of salinity as limiting factor and environmental control of microbial mat function at more hypersaline conditions.

Compared to the well-studied hypersaline mats from Solar Lake (Egypt), Guerrero Negro (Mexico) and Storrs Lake (Bahamas), which normally experience relatively constant salinity conditions, microbial mats in a saltern in Puerto Rico experience strong annual salinity fluctuations, with a typical pattern of dry and wet seasons of the tropical Caribbean (Casillas-Martinez *et al*., 2005). Casillas-Martinez *et al*. (2005) showed that in response to this natural salinity increase from 40 to 265 between both seasons, the community composition and geochemical and microbial indices (metabolic activity, solute distribution, chlorophyll *a*) changed significantly. Despite decreasing rates at higher salinities, the community remained relatively active at the high salinity conditions when chlorophyll *a*-normalized photosynthesis rates were compared. Thus, also this microbial mat community appears extremely well adapted to its naturally fluctuating environment, determining the extent of halotolerance of the microbial community.

For moderately hypersaline conditions, it is remarkable, that *Microcoleus*-dominated mats from different geographic location [(Laguna Guerrero Negro (Mexico), Spencer Gulf (Australia), Camargue (France)] show a broad salinity tolerance of light-saturated photosynthesis (Bauld, 1984; Javor & Castenholz, 1984; this study). Comparable to our results, *Microcoleus*-mats in high intertidal areas of Spencer Gulf (South Australia) showed maximum photosynthetic activity between $S = 70$–105 in early summer (Bauld, 1984) and are apparently also well adapted to the prevailing natural fluctuating salinities. Further, *Microcoleus*-mats growing in the solar salterns of Guerrero Negro (Mexico) at $S = 90$ and 120, which were transferred and maintained in a greenhouse facility at both salinities showed no differences of oxygen microprofiles and net photosynthesis rates during daytime (Bebout *et al*., 2002).

Studies of the salinity-effects on photosynthesis in selected *Microcoleus*-mats (Bauld, 1984; Garcia-Pichel *et al*., 1999; this study) and in *Microcoleus*-mats along a salinity gradient (Des Marais *et al*., 1989) show clearly that at salinities higher than ~100 photosynthetic activity decreases in *Microcoleus*-dominated mats independent of the respective community composition and geographical habitat location. This correlates well with the salinity range in which *Microcoleus*-dominated mats flourish (~60–120). *M. chthonoplastes* decreases strongly in abundance at salinities above 150, with increasing abundance of species of other cyanobacterial genera apparently better adapted to higher osmotic stress (reviewed in Oren, 2000). Thus, the dominating cyanobacterium in these mats obviously determines the salinity response of the overall phototrophic mat community within this moderately hypersaline salinity range.

Our findings of a pronounced role of temperature within the salinity range of natural variations (and in which *M. chthonoplastes* dominated mats flourish in general) can hence be explained by the broad salinity tolerance of the Camargue mats and may also apply for *Microcoleus*-mats in environments with strongly fluctuating salinities as, e.g. in upper intertidal areas. *Microcoleus*-mats growing under more constant environmental conditions (see above) may show a stronger dependency of activity on salinity changes. A strong increase of light-saturated photosynthesis with temperature and an optimum at elevated temperatures (30–40 °C) is generally found for *Microcoleus*-dominated mats (e.g. Javor & Castenholz, 1984; Canfield & Des Marais, 1993; Epping & Kühl, 2000; Wieland & Kühl, 2000a, b). At more hypersaline conditions, however, the role of salinity increases and finally overrides in determining mat community function, leading to reduced metabolic activity and changes of microbial composition, biodiversity and structure of mats.

In conclusion, the investigated microbial mat community is apparently well adapted to short-term variations of salinity and only salinity extremes (relative to the *in situ* level) led to a pronounced change in O_2 turnover rates. This indicates an increasing importance of salinity as limiting parameter at increasing hypersaline conditions. Effects on physical parameters and mass transfer contributed to the response of dark oxygen consumption rates to changes of environmental parameters, which was most pronounced at increasing temperature. Within the range of natural variation under moderately hypersaline conditions, temperature was a more important regulating environmental parameter than salinity for photosynthetic activity and O_2-consuming processes in the Camargue microbial mat. However, microbial mats from different settings may exhibit different responses to short-term changes of key environmental parameters, determined by the variability and the range of these parameters in their habitat. It may not be possible to generalize results from the investigation of a specific microbial mat community to other mats growing in hypersaline environments, e.g. under more stable conditions or at higher *in situ* salinities. In fact, there is a need for a systematic investigation and comparison of microbial mat communities from settings with fluctuating and more constant temperature and salinity conditions to further resolve the microenvironmental controls acting in these fascinating ecosystems.

Acknowledgements

We acknowledge financial support by the EU (contract no. EVK3-CT-1999-00010 and QLK3-CT-2002-01938), the Danish Natural Science Research Council (M.K.), and the German Science Foundation (A.W.). The salt company Salins-du-Midi in Salin-de-Giraud, France, is gratefully acknowledged for access to the field site. Anni Glud is thanked for construction of microsensors and Gerard Versteegh for valuable discussions.

References

Bauld J (1984) Microbial mats in marginal marine environments: Shark Bay, Western Australia, and Spencer Gulf, South Australia. *Microbial Mats: Stromatolites* (Cohen Y, Castenholz RW & Halvorson HO, eds), pp. 39–58. Alan R. Liss, New York.

Bebout BM, Carpenter SP, Des Marais DJ, *et al.* (2002) Long-term manipulations of intact microbial mat communities in a greenhouse collaboratory: simulating earth's present and past field environments. *Astrobiol* **2**: 383–402.

Benthien M, Wieland A, García de Oteyza T, Grimalt JO & Kühl M (2004) Oil-contamination effects on a hypersaline microbial mat community (Camargue, France) as studied with microsensors and geochemical analysis. *Ophelia* **58**: 135–150.

Boudreau BP & Jørgensen BB (2001) *The Benthic Boundary Layer: Transport Processes and Biogeochemistry*. Oxford University Press, Oxford.

Canfield DE & Des Marais DJ (1993) Biogeochemical cycles of carbon, sulfur, and free oxygen in a microbial mat. *Geochim Cosmochim Acta* **57**: 3971–3984.

Canfield DE, Sørensen KB & Oren A (2004) Biogeochemistry of a gypsum-encrusted microbial ecosystem. *Geobiol* **2**: 133–150.

Casillas-Martinez L, Gonzalez ML, Fuentes-Figueroa Z, Castro CM, Nieves-Mendez D, Hernandez C, Ramirez W, Sytsma RE, Perez-Jimenez J & Visscher PT (2005) Community structure, geochemical characteristics and mineralogy of a hypersaline microbial mat. Cabo Rojo. PR. *Geomicrobiol J* **22**: 269–281.

Davison IR (1991) Environmental effects on algal photosynthesis: temperature. *J Phycol* **27**: 2–8.

Des Marais DJ, Cohen Y, Nguyen H, Cheatham M, Cheatham T & Munoz E (1989) Carbon isotopic trends in the hypersaline ponds and microbial mats at Guerrero Negro, Baja California Sur, Mexico: implications for precambrian stromatolites. *Microbial Mats. Physiological Ecology of Benthic Microbial Communities* (Cohen Y & Rosenberg E, eds), pp. 191–203. American Society for Microbiology, Washington, DC.

Epping E & Kühl M (2000) The responses of photosynthesis and oxygen consumption to short-term changes in temperature and irradiance in a cyanobacterial mat (Ebro Delta, Spain). *Environ Microbiol* **2**: 465–474.

Fourçans A, García de Oteyza T, Wieland A, *et al.* (2004) Characterization of functional groups in a hypersaline microbial mat community (Salins-de-Giraud, Camargue, France). *FEMS Microbiol Ecol* **51**: 55–70.

Galinski EA (1993) Compatible solutes of halophilic eubacteria: molecular principles, water-solute interactions, stress protection. *Experientia* **49**: 487–496.

Galinski EA (1995) Osmoadaptation in bacteria. *Adv Microb Physiol* **37**: 273–328.

Galinski EA & Trüper HG (1994) Microbial behaviour in salt-stressed ecosystems. *FEMS Microbiol Rev* **15**: 95–108.

Garcia-Pichel F, Kühl M, Nübel U & Muyzer G (1999) Salinity-dependent limitation of photosynthesis and oxygen exchange in microbial mats. *J Phycol* **35**: 227–238.

Golubic S (1980) Halophily and halotolerance in cyanophytes. *Origins of Life* **10**: 169–183.

Hancke K & Glud RN (2004) Temperature effects on respiration and photosynthesis in three diatom-dominated benthic communities. *Aquat Microb Ecol* **37**: 265–281.

Henley WJ (1993) Measurement and interpretation of photosynthetic light-response curves in algae in the context of photoinhibition and diel changes. *J Phycol* **29**: 729–739.

Isaksen MF & Jørgensen BB (1996) Adaptation of psychrophilic and psychrotrophic sulfate-reducing bacteria to permanently cold marine environments. *Appl Environ Microbiol* **62**: 408–414.

Jørgensen BB & Des Marais DJ (1990) The diffusive boundary layer of sediments: oxygen microgradients over a microbial mat. *Limnol Oceanogr* **35**: 1343–1355.

Jørgensen BB & Revsbech NP (1985) Diffusive boundary layers and the oxygen uptake of sediments and detritus. *Limnol Oceanogr* **30**: 111–122.

Javor BJ & Castenholz RW (1984) Productivity studies of microbial mats, Laguna Guerrero Negro, Mexico. *Stromatolites* (Cohen Y, Castenholz RW & Halvorson HO, eds), pp. 149–170. Alan R. Liss, Inc., New York.

Joint I, Henriksen P, Garde K & Riemann B (2002) Primary production, nutrient assimilation and microzooplankton grazing along a hypersaline gradient. *FEMS Microbiol Ecol* **39**: 245–257.

Joset F, Jeanjean R & Hagemann M (1996) Dynamics of the response of cyanobacteria to salt stress: deciphering the molecular events. *Physiol Plant* **96**: 738–744.

Karsten U (1996) Growth and organic osmolytes of geographically different isolates of *Microcoleus chthonoplastes* (cyanobacteria) from benthic microbial mats: response to salinity change. *J Phycol* **32**: 501–506.

Lajkó F, Kadioglu A, Borbély G & Garab G (1997) Competition between the photosynthetic and the (chloro)respiratory electron transport chains in cyanobacteria, green algae and higher plants. Effect of heat stress. *Photosynthetica* **33**: 217–226.

Lorenzen J, Glud RN & Revsbech NP (1995) Impact of microsensor-caused changes in diffusive boundary layer thickness on O_2 profiles and photosynthetic rates in benthic communities of microorganisms. *Mar Ecol Prog Ser* **119**: 237–241.

Oren A (1990) Formation and breakdown of glycine betaine and trimethylamine in hypersaline environments. *Antonie van Leeuwenhoek* **58**: 291–298.

Oren A (1999) Bioenergetic aspects of halophilism. *Microb Mol Biol Rev* **63**: 334–348.

Oren A (2000) Salts and Brines. *The Ecology of Cyanobacteria* (Whitton BA & Potts M, eds), pp. 281–305. Kluwer, Dordrecht.

Paerl HW, Steppe TF, Buchan KC & Potts M (2003) Hypersaline cyanobacterial mats as indicators of elevated tropical Hurricane activity and associated climate change. *Ambio* **32**: 87–90.

Peschek GA (1999) Photosynthesis and respiration of cyanobacteria. *The Phototrophic Prokaryotes* (Peschek GA, Löffelhardt W & Schmetterer G, eds), pp. 201–209. Kluwer, New York.

Pinckney J, Paerl HW & Bebout BM (1995) Salinity control of benthic microbial mat community production in a Bahamian hypersaline lagoon. *J Exp Mar Biol Ecol* **187**: 223–237.

Reed RH, Warr SRC, Kerby NW & Stewart WDP (1986) Osmotic shock-induced release of low molecular weight metabolites from free-living and immobilized cyanobacteria. *Enzyme Microb Technol* **8**: 101–104.

Revsbech NP (1989) An oxygen microelectrode with a guard cathode. *Limnol Oceanogr* **34**: 474–478.

Revsbech NP & Jørgensen BB (1983) Photosynthesis of benthic microflora measured with high spatial resolution by the oxygen microprofile method: capabilities and limitations of the method. *Limnol Oceanogr* **28**: 749–756.

Riley JP & Skirrow G (1975) *Chemical Oceanography*, pp. 338. Academic Press, London.

Roeßler M & Müller V (2001) Osmoadaptation in Bacteria and Archaea: common principles and differences. *Environ Microbiol* **3**: 743–754.

Sørensen KB, Canfield DE & Oren A (2004) Salinity responses of benthic microbial communities in a solar saltern (Eilat, Israel). *Appl Environ Microbiol* **70**: 1608–1616.

Sherwood JE, Stagnitti F, Kokkinn MJ & Williams WD (1991) Dissolved oxygen concentrations in hypersaline waters. *Limnol Oceanogr* **36**: 235–250.

Skyring GW & Bauld J (1990) Microbial mats in Australian coastal environments. *Adv Microb Ecol* **19**: 461–498.

Stal LJ (2000) Cyanobacterial mats and stromatolites. *The Ecology of Cyanobacteria* (Whitton BA & Potts M, eds), pp. 61–120. Kluwer, Dordrecht.

Ventosa A, Nieto JJ & Oren A (1998) Biology of moderately halophilic aerobic bacteria. *Microbiol Mol Biol Rev* **62**: 504–544.

Webb WL, Newton M & Starr D (1974) Carbon dioxide exchange of *Alnus rubra*: a mathematical model. *Oecologia* **17**: 281–291.

Wieland A & Kühl M (2000a) Irradiance and temperature regulation of oxygenic photosynthesis and O_2 consumption in a hypersaline cyanobacterial mat (Solar Lake, Egypt). *Mar Biol* **137**: 71–85.

Wieland A & Kühl M (2000b) Short-term temperature effects on oxygen and sulfide cycling in a hypersaline cyanobacterial mat (Solar Lake, Egypt). *Mar Ecol Prog Ser* **196**: 87–102.

Wieland A & Kühl M (2001) Oxygen cycling in microbial mats from Camargue (France), Ebro Delta (Spain) and mesocosms (Eilat, Israel). *Proceedings of the first MATBIOPOL project meeting in Marseilles (France)*, 25–42.

Wieland A, Zopfi J, Benthien M & Kühl M (2005) Biogeochemistry of an iron-rich hypersaline microbial mat (Camargue, France). *Microb Ecol* **49**: 34–49.